KLVFF Oligopeptide-Decorated Amphiphilic Cyclodextrin Nanomagnets for Selective Amyloid Beta Recognition and Fishing

Antonino Mazzaglia,[a*] Giuseppe Di Natale,[b] Rita Tosto,[b, c] Angela Scala,[d] Giuseppe Sortino,[a] Anna Piperno,[d] Maria Pia Casaletto,[e] Alberto Riminucci,[f] Placido G. Mineo,[g] Valentina Villari,[h] Norberto Micali[h*] and Giuseppe Pappalardo[b*]

[a] Consiglio Nazionale delle Ricerche, Istituto per lo Studio dei Materiali Nanostrutturati (CNR-ISMN), c/o Dipartimento di Scienze Chimiche, Biologiche, Farmaceutiche ed Ambientali, Università di Messina, Viale F. Stagno D'Alcontres 31, 98166 Messina, Italy

[b] Consiglio Nazionale delle Ricerche, Istituto di Cristallografia (CNR-IC), Via P. Gaifami 18, 95126 Catania, Italy

[c] International PhD School of Chemical Sciences, University of Catania, 95125 Catania, Italy

[d] Dipartimento di Scienze Chimiche, Biologiche, Farmaceutiche ed Ambientali, Università di Messina, Viale F. Stagno d'Alcontres 31, Messina 98166, Italy

[e] Consiglio Nazionale delle Ricerche, Istituto per lo Studio dei Materiali Nanostrutturati (CNR-ISMN), Via U. La Malfa, 153, 90146 Palermo, Italy

[f] Consiglio Nazionale delle Ricerche, Istituto per lo Studio dei Materiali Nanostrutturati (CNR-ISMN), Via P. Gobetti 101, 40129 Bologna, Italy

[g] Dipartimento di Scienze Chimiche, Università di Catania, V. le A. Doria 6, 95125 Catania, Italy

[h] Consiglio Nazionale delle Ricerche, Istituto per i Processi Chimico-Fisici (CNR-IPCF), Viale F. Stagno D'Alcontres 37, 98158 Messina, Italy.

ABSTRACT

Recognition and capture of amyloid beta (Aβ) is a challenging issue in the early diagnosis of neurodegenerative disorders, such as Alzheimer's disease (AD). Here, we report on novel nanoassemblies based on magnetic nanoparticles (MNP) covered with a non-ionic amphiphilic β-cyclodextrin (aCD, SC16OH) and decorated with KLVFF peptide for the self-recognition of the homologous amino-acids sequence of Aβ and recruiting of the toxic form Aβ (1-42). SC16OH was synthesized by modifying CD primary side with thiohexadecyl chain and the secondary rim

with poly-ethylene glycol arms bearing in average 4-5 units of ethylene oxide for glucose unit. MNP@SC16OH nanoassemblies were prepared in water by mixing pre-formed SC16OH nanovesicles with MNP followed by magnet settling and freeze-drying. The nanoassemblies were characterized by TGA, XPS and magnetization measurements. The capping reaction afforded an aCD coverage of ~ 22% w/w and, at an applied field of 1 kOe, MNP@SC16OH exhibited a slight decrease of mass magnetization (36 emu/g) *vs* naked MNP (48 emu/g). Adamantyl-$(PEG)_4$-KLVFF (Ada-Pep) was incorporated in MNP@SC16OH with a loading of about 5.3 % w/w (corresponding to 48 nmoles/mg of MNP@SC16OH/Ada-Pep) by supramolecular interaction between CD cavities and the adamantyl moieties, with the aim to expose the KLVFF peptide on the nanomagnets surface. TEM analysis showed the presence of single domain MNP@SC16OH/Ada-Pep nanomagnets of 20-40 nm. DLS and ζ-potential measurements revealed that MNP@SC16OH nanoassemblies owned in aqueous dispersion a hydrodynamic radius (R_H) of about 150 nm, which was unaffected by Ada-Pep decoration, while the negative ζ-potential of MNP@SC16OH (-35 mV) became less negative (-30 mV) in MNP@SC16OH/Ada-Pep, confirming the exposition of positively charged KLVFF on nanomagnets surface.

The ability of MNP@SC16OH/Ada-Pep to recruit Aβ (1-42) in aqueous solution was evaluated by MALDI-TOF and compared with the ineffectiveness of undecorated MNP@SC16OH and VFLKF scrambled peptide-decorated nanoassemblies (MNP@SC16OH/Ada-*sc*Pep), pointing out the selectivity of KLVFF-decorated nanohybrid towards Aβ (1-42).

Keywords: amphiphilic cyclodextrins, nanovesicles, magnetic nanoparticles, beta amiloid, molecular recognition, MALDI-TOF analysis, oligopeptides, nanoassemblies, hybrid aggregates, fishing

1. INTRODUCTION

Over the past decade, magnetic nanoparticles (MNP) have been identified as versatile tools in biomedical applications ranging from sensing and detection of biomarkers to imaging, therapy and theranostic.[1-6]A variety of covering agents, including polymers, macrocycles, dendrimers etc., linked or adsorbed on MNP surface, confer them biocompatibility and biodegradability for *in vitro*

and *in vivo* treatments.[7-10] Due to their unique structural properties, such as the tunable core size and large surface to volume ratio, functionalised MNP possess the capability to bind proteins and cells.[11]Alzheimer's disease (AD) is a widespread neurodegenerative disorder, characterized by a progressive failure in cognitive function and by memory loss.[12] The aggregation of amyloid beta (Aβ) peptides, whose major representative are the neurotoxic polypeptides Aβ (1-40) and Aβ (1-42), is an event occuring at the early stages of AD.[13] Such a pathological phenomenon can lead eventually to the formation of the so-called Aβ plaques, that have been validated as an AD hallmark.[14]

The quantification of Aβ oligomers in cerebrospinal fluid (CSF) and, specifically, the Aβ (1-42) to Aβ (1-40) peptide ratio was proposed for the early AD diagnosis and to monitor the disease progression, although the low level of oligomers in CSF made their reliable quantification challenging. However, the reputed value of Aβ in the pathological processes should be further evaluated and consolidated since the overlapping of AD with other forms of dementia and the limits of the current detection methods (*i.e.,* ELISA, Western Blot, ultrasensitive bead-based immunoassays) can cause controversial results.[15]

Miniaturized magnetic devices at micro and nano-scale level have been widely exploited for sensing and recognition of Aβ.[16-19] MNP modified with anti-biofouling,[20] fluorescent,[21-23] plasmonic[24] or scavenging[25]nanolabels have been proposed to detect Aβ and/or inhibit its abnormal aggregation in Aβ plaques or even to clean Aβ from blood.[26] Among these, MNP modified with antibodies,[11,22] aptamers[23] or oligopeptides[21,26] have shown high selectivity in recognition of monomeric or aggregates amyloid species and/or in their disaggregation.

The hydrophobic pentapeptide KLVFF (H_2N-Lys-Leu-Val-Phe-Phe-COOH, Aβ (16-20), see Scheme 1), is the self-recognition sequence of the homologous amino acids sequence both in Aβ (1-40) [27] and in the more toxic form Aβ (1-42),[28] and is known to be the fragment responsible of the nucleation of protofibrillar Aβ and further aggregation.[29] Due to its recognition leading role, this amino acid sequence could inhibit the aggregation into fibrils by disassembly of the preformed aggregates.[29] Many variants of this sequence have been synthetized and studied as peptide-based drugs for the treatment of Alzheimer's disease.[30]

Accordingly, a variety of metal nanoparticles conjugates with KLVFF or other peptides exhibited properties in terms of inhibition and/or recognition of Aβ alloforms[28,31] and deposits.[32]

Cyclodextrins (CDs) are cyclic oligosaccharides with high capacity of entrapping hydrophobic guest in their cavity or interacting outside the cavity with hydrophilic species.[33] CDs coupled with specific binding peptides and/or nanoparticles served extensively for helping in the capture, detection and disintegration of Aβ fibrils.[34-37] Such nanostructured hybrid materials bearing both organic and inorganic components have attracted attention due to the possibility of tailoring their abilities in function of a desired responsiveness. As an example, in the field of biomedical research, numerous CD-modified MNP have been proposed as hybrid nanoassemblies for tumor therapy,[38-40] although few reports have concerned their utilize in biosensing.[41] Recently, the electrosensing of bio-target by CD vesicles hosting MNP (e.g superparamagnetic nanoparticles, SPION) has been reported.[42] CD-modified MNP are less explored in AD research and only rare reports deal with the interaction of CD/MNP hybrids with Aβ peptides.[43] In the framework of this ongoing research, recently various inorganic/organic hybrid platform based on CD were explored in our groups for biomedical purposes.[44-47] Also hybrid self-assemblies based on amphiphilic CD (aCD) have been proposed as nano-therapeutics[48] or to inhibit amyloid fibrillation.[49] A fine-tuning of the physico-chemical properties, such as molar ratio of metal/covering agent, selection of entrapped drug and/or fluorescent probe and decoration with targeting agents, is highly desirable for the nanocontruct engineering to improve the payload delivery and/or recognition of cell receptors.[50] The ability to control the supramolecular organization of the composite nanostructures is also required for the effectiveness of the designed device. Our strategy explores most of the latter properties together with the utilize of a specific oligopeptide motif which confers to nanomagnets recognition ability for Aβ peptides. Accordingly, we newly design and fully characterize a KLVFF-modified nanomagnet based on magnetite nanoparticles (Fe_3O_4; MNP) capped by an amphiphilic CD shell (SC16OH) for capture of Aβ peptides in aqueous medium. KLVFF oligopeptide was conjugated to adamantane through a pegylated arm leading to Adamantanyl-$(PEG)_4$-KLVFF (Ada-Pep) with the aim to exploit the high binding constant of adamantane for CD cavity ($K_b \approx 10^5\ M^{-1}$).[45, 46, 50, 51]Therefore, on one end, Ada-Pep was anchored on the macrocyclic by supramolecular interaction[50, 52] so that on the other side the recognition domain was exposed on the nanomagnet surface (Scheme 1). MNP@SC16OH and MNP@SC16OH/Ada-Pep nanoassemblies were fully characterized by complementary techniques both as solid powders and in aqueous dispersions. Finally, MALDI-TOF analysis was employed to validate the capability of MNP@SC16OH/Ada-Pep in catching out Aβ (1-42) from aqueous solutions. Adamantanyl-

$(PEG)_4$-VFLKF- (Ada-*sc*Pep) decorated nanomagnets bearing the scrambled peptide VFLKF were used as as negative control (see Scheme1).

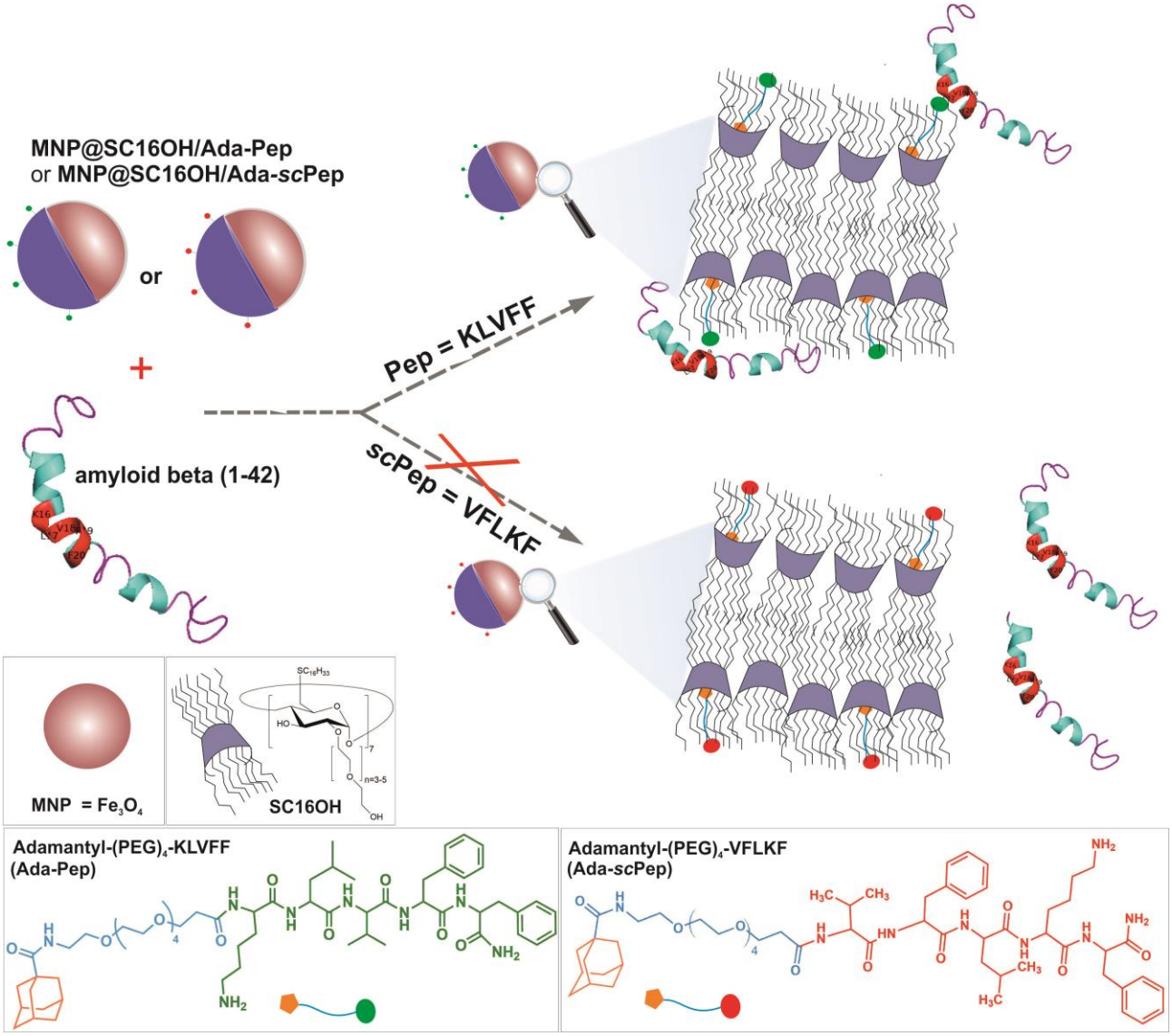

Scheme 1. Sketched view of oligopeptide-decorated amphiphilic cyclodextrin nanomagnets (MNP@SC16OH/Ada-Pep and MNP@SC16OH/Ada-*sc*Pep) with the structures of Adamantyl-$(PEG)_4$-KLVFF (Ada-Pep) and Adamantyl-$(PEG)_4$-VFLKF (Ada-*sc*Pep) and the interaction arrangement of

MNP@SC16OH/Ada-Pep recruiting amyloid beta (1-42), Aβ (1-42), *vs* ineffective MNP@SC16OH/Ada-*sc*Pep.

2. EXPERIMENTAL SECTION

Chemicals and Materials

All solvents and reagents were obtained from commercial sources and purified before use if necessary. Merck Kieselgel 60F254 plates were used for TLC, and Sephadex LH-20 for column chromatography. Iron(II,III) oxide nanopowder (MNP) and β-Cyclodextrin were purchased by Merck (Italy). All the solutions for spectroscopic characterization were prepared in ultrapure water (Galenica Senese) and analyzed at room temperature (r.t ~ 25°C). Millipore Milli-Q purified water (milliQ water) was used for analysis by MALDI-TOF mass spectra (MALDI-TOF-MS).

Synthesis of Heptakis[6-deoxy-6-hexadecylthio-2-poly(ethylene glycol)]-β-cyclodextrin (SC16OH). SC16OH was synthesized by a slightly modified procedure.[53] Briefly, heptakis(6-deoxy-6-hexadecylthio)-β-cyclodextrin (1.54 g, 0.5 mmol), potassium carbonate (K_2CO_3, 2 molar equiv.) and ethylene carbonate (60 molar equiv.) were dissolved in 10 mL of tetramethylurea. The mixture was stirred at 150°C under nitrogen for 5 h followed by stirring at room temperature (r.t.) for further 16 h. The solvent was removed under vacuum at 100°C and the crude was treated with 0.1 M sodium methoxide in methanol (MeOH) at 65°C for 3 h. The product was purified by size-exclusion chromatography using a 1:1 chloroform:MeOH mixture as eluent, to obtain SC16OH as a powder. Yield: 47%.

^{1}H NMR (500 MHz, CDCl3): δ = 0.88 (t, 21 H, CH3), 1.26 (br s, 182 H, CH2), 1.51-1.60 (m, 14 H, CH2), 1.74 (br, OH), 2.52-2.60 (m, 14 H, SCH2), 2.93-3.06 (m, 14 H, H6), 3.27-4.00 (m, ca. 132 H , H2-5 and OCH2CH2O), 5.07 (br, 7 H, H1). ^{13}C NMR (125 MHz, CDCl3): δ = 14.1 (CH3), 22.5 (CH2), 28.5 (CH2), 29.1 (CH2), 29.4 (CH2), 29.5 (CH2), 29.7 [(CH2)n], 31.9 (SCH2), 33.7 (C6), 61.4 (CH2OH), 69.8-74.5 (C3, C5, CH2O), 80.1-82.4 (C2, C4), 101.1 (C1). Average molecular weights determined by MALDI-TOF-MS:[54-56] Mw=4224 Da; Mn=3974 Da; PDI=1.063. At the most abundant peak, the average number (n) of ethylene oxide units (EO) resulted equal to 32.

Synthesis of Adamantyl-(PEG)$_4$-KLVFF (Ada-Pep) and Adamantyl-(PEG)$_4$-VFLKF (Ada-scPep). Peptides, both KLVFF (Pep) and VFLKF (scrambled Pep, *sc*Pep), were synthesised on a Liberty Peptide Synthesizer (CEM) according to microwave-assisted solid-phase peptide synthesis.[57] The synthesis was carried out using a NovaSyn TGR resin (substitution 0,22 mmol/g) as a solid support. The Fmoc/tBut chemistry was used. Fmoc-amino acids were linked to the growing peptide chain using 1-[(1-(cyano-2-ethoxy-2-oxoethylideneamino- oxy)-dimethylamino-morpholinomethylene)] methanaminium hexafluorophosphate (COMU) as a condensing agent.[58] (PEG)$_4$ and adamantyl were inserted by a double coupling cycle using Fmoc-15-amino-4,7,10,13-tetraoxapentadecacanoicacid (Fmoc-(PEG)$_4$) and adamantane-carboxylic acid (Ada-COOH) as reagents. Each amino acid coupling was carried out under a four-fold excess. Removal of the Fmoc protection during synthesis was achieved by means of 20 % piperidine solution in N,N-Dimethylformamide (DMF). The following instrumental conditions were used for each coupling cycle: microwave power 25 Watts, reaction temperature 75 °C, coupling time 300 s. The instrumental conditions used for the deprotection cycles were: microwave power 25 Watts, reaction temperature 75°C, deprotection time 180 s. The peptides were cleaved off from the resin using a mixture of Tifluoroacetic acid/Water/ Triisopropylsilane (TFA/H_2O/TIS, 95:2.5:2.5 v/v/v). Crude peptides were recovered by precipitation with freshly distilled diethyl ether. The purification of crude peptides was carried out by preparative reversed-phase HPLC using a SHIMADZU LC-20A chromatography system equipped with an SPD-M20A photodiode diode array detector with detection at 222 and 254 nm. A Kinetex C18 250 × 21.10 mm (100 Å pore size, AXIA Packed) column was used. The peptides were eluted at a flow rate of 10 mL/min according to the following protocol: from 0 to 5 min isocratic conditions in 90% solvent A (H_2O containing 0.1 % TFA) followed by a 20 min linear gradient from 10 to 80% B , acetonitrile (CH_3CN) containing 0.1 % TFA, and then 5 min isocratic conditions in 80 % B (R_t=18min). Fractions containing the desired product were collected and lyophilized. The identity of the synthesized peptides was confirmed by MALDI-TOF-MS. Calculated mass 1104.7; Observed for Adamantyl-(PEG)$_4$-KLVFF (Ada-Pep) : $[M+H]^+$ = 1105.84; $[M+Na]^+$ = 1127.99 ; for Adamantyl-(PEG)$_4$-VFLKF (Ada-*sc*Pep) $[M+H]^+$ = 1105.86; $[M+Na]^+$ = 1127.99. $[M+2H]^{2+}$ = 553.67.

Preparation of MNP@SC16OH nanomagnets.An aqueous dispersion of SC16OH nanovesicles (1.2 mg/mL) was prepared as previously reported.[59,60] Briefly, SC16OH (15 mg) was dissolved in dichloromethane (DCM, 2 mL) and the solvent was evaporated overnight. The organic layer was hydrated with ultrapure water (12.5 mL) at T≅ 50°C and sonicated by microtip probe (UW 2070 SONOPULS, Bandelin Electronic, Berlin, Germany) with a 35% power for 90 min by using an ice bath and equilibrated at r.t.. MNP@SC16OH were prepared by mixing MNP (15 mg) with the aqueous dispersions of SC16OH (1.2 mg/mL, V=12.5 mL) under argon. The dispersion was left stirring at r.t. for 72 h. MNP@SC16OH were isolated by magnet settling for 48 h. The supernatants were separated from residues and subjected to further settling by magnet for 24 h. All the magnetic powders were collected together, washed with ultrapure water and separated by magnet settling once again. Hence, MNP@SC16OH was dried at 60°C under vacuum and isolated as a dark brown powder (recovery yield about 63 w/w %).

Preparation of MNP@SC16OH/Ada-Pep and MNP@SC16OH/scAda-Pep nanomagnets. A stock solution of Ada-Pep or Ada-*sc*Pep (1 mM) was prepared dissolving 1.13 mg of powder in DCM/MeOH (97:3 v/v) and used to prepare an organic film of Ada-Pep or Ada-*sc*Pep (78 μM). MNP@SC16OH/Ada-Pep and MNP@SC16OH/Ada-*sc*Pep, at about 1:1 molar ratio ([SC16OH] = [Ada-Pep] or [Ada-*sc*Pep] = 78 μM, 0.377 μmoles) were prepared by hydration of the organic film (Ada-Pep or Ada-*sc*Pep) with a pre-sonicated (~ 2 h) aqueous solution of MNP@SC16OH (7.2 mg, V=4.84mL) followed by a first sonication in ultrasonic bath for about 30 minutes, and then for about 3h by a microtip probe sonicator under ice-cooling (*see above).* The final dispersion was stored at 4°C overnight. Afterward, MNP@SC16OH/Ada-Pep or MNP@SC16OH/Ada-*sc*Pep was precipitated by magnet settling and centrifuged at 6000 RPM for 20 minutes. The supernatant was removed and the solid powder was washed and centrifuged again and then freeze-dried.

Peptide loading. An indirect method to evaluate the loading of Ada-Pep in MNP@SC16OH/Ada-Pep was used calculating the difference between the initial amount of Ada-Pep (377 nanomoles) and the concentration of residual Ada-Pep in the supernatant after its incorporation in the nanomagnets, determined by MALDI-TOF-MS.

Ada-Pep actual loading (AL%), theoretical loading (TL%) and entrapment efficiency percentages (EE%) were evaluated as follows:

$$AL\ (\%) = \frac{amount\ of\ initial\ Ada-Pep-\ amount\ of Ada-Pep\ \ in\ the\ supernatant}{weight\ of\ nanomagnets} \times 100 \quad (1)$$

$$TL\ (\%) = \frac{amount\ of\ initial\ Ada-Pep}{weight\ of\ nanomagnets} \times 100 \quad (2)$$

$$EE\ (\%) = \frac{amount\ of\ initial\ Ada-Pep\ -\ amount\ of\ Ada-Pep\ \ in\ the\ supernatant}{amount\ of\ initial\ Ada-Pep} \times 100 \quad (3)$$

Calibration curves of the standard Ada-Pep solutions were constructed by analyzing the data from MALDI–TOF-MS. Standard solutions were prepared in the concentration range 1.0-10.0 μM.

Monoisotopic peaks were automatically detected using a freely available open-source software, mMass (http://www.mmass.org). The m/z signal intensities were exported as peaks list and processed by excel (Microsoft) software. The linear standard curve and the relative correlation coefficient was reported in Figure S1.

Methods

Mass spectrometry. MALDI-TOF-MS of SC16OH were acquired with a Voyager DE (PerSeptive Biosystem) equipped with a delay extraction device (see SI).[54-56]

Electrospray mass spectra (ESI-MS) of peptides conjugates (Ada-Pep and Ada-*sc*Pep) were recorded on a Finnigan LCQ-DECA ion trap electrospray mass spectrometer (see SI).

Thermogravimetric analysis (TGA). The analyses were conducted using a Perkin-Elmer TGA 7 and a TAC 7/DX (thermal ramp of 10 °C min^{-1}) in the range 50-800°C, in air atmosphere (60 mL min^{-1}).

X-Ray Photoelectron Spectroscopy (XPS). XPS spectra were acquired by using a VG Microtech ESCA3000 Multilab spectrometer, equipped with a twin anode X-Ray source (Mg and Al) and a five channeltrons detection system (see SI).

Magnetic characterization. A custom-built Faraday magnetometer was used to measure the samples' specific moment σ (i.e. the magnetic moment per unit mass) as a function of the applied field at 27°C.[61] The magnetometer is based on a Sartorius ME235S analytical balance and a NdFeB permanent magnet, with a maximum applied magnetic field of approximately 0.12 T.

Dynamic Light Scattering and Electrophoretic Light Scattering. Dynamic Light Scattering (DLS) was performed by a homemade apparatus.[62] The particle size was obtained by means of the scattered intensity correlation function. The wavelength used was 632 nm (35mW HeNe laser) and the scattered light was detected in a self-beating mode at the scattering angle of 90°. For the data analysis, we used the Laplace inversion algorithm in order to obtain the distribution of relaxation times and the cumulant analysis to obtain the average hydrodynamic radius. The electrophoretic mobility (μ) of the colloidal samples, and hence the zeta potential value (ζ-potential), was measured by using a ZetaPALS instrument (Brookhaven) which is based on the principle of the Phase Analysis Light Scattering. For DLS and ζ-potential measurements MNP, MNP@SC16OH and MNP@SC16OH/Ada-Pep were prepared by dissolving the freeze dried powder in ultrapure water (0.16 mg/mL), sonicated by a microtip probe sonicator (*see above*) under ice-cooling (20 min) and equilibrated at r.t.

Trasmission Electron Microscopy (TEM). Morphology of MNP@SC16OH/Ada-Pep was investigated at University of Exeter (UK) using a TEM, JEM2100 LaB6, working at 200 kV, and a digital Scanning transmission electron microscopy (STEM) equipped with BF & DF STEM Detectors plus SE/BSE detector.[63] Samples for TEM and STEM were prepared by placing 8-10 drops of pre-sonicated (about 3 h in ultrasound bath) dispersion in ultrapure water (~0.1 mg/mL) on 300 mesh holey-carbon coated copper grids. Atomic force microscopy (AFM) was carried out by Bruker Innova working in magnetic mode with sub-nanometer resolution.[64]

Fishing protocol. The Aβ (1-42) monomerization was accomplished using the following procedure. The peptide was dissolved in TFA (1 mg mL^{-1}) and sonicated in a water bath for 10 min. Then the solvent was evaporated under a gentle stream of argon and 1 mL of hexafluoroisopropanol (HFIP) was added to the resulting peptide film. After 1 h incubation at 37°C, the peptide solution was dried under a stream of argon and the residual was dissolved in 2

mL of HFIP. The solution was dried with an argon stream to remove the remaining trace of TFA and the sample was again dissolved in 1 ml HFIP and frozen at −30°C. The iced solution was lyophilized overnight. The lyophilized sample was dissolved in milliQ water, to obtain a concentration of $2.2x10^{-4}$ M (stock solution). Samples of Aβ (1-42) were prepared from stock solutions to a final concentration of 10 μM. Each sample (300 μL) was incubated at room temperature for 24 h with 1 mg of different MNPs, namely MNP@SC16OH/Ada-Pep, and MNP@SC16OH/*sc*Ada-Pep and MNP@SC16OH as controls. After incubation the supernatant was removed (incubation fraction) from the nanoparticles (NPs) by magnetic settling. Hence nanoparticles were washed three times in 300 μL of milliQ water (washing fraction). Next, NPs were suspended in 300 μL of DCM/CH_3CN 97/3, and sonicated in a water bath for 10 min. The supernatant was separated from NPs, dried under Nitrogen steam and solubilized in HFIP (extraction fraction). Afterwards, each solution (incubation fraction, washing fraction and extraction fraction) was frozen at −30 °C and the iced solutions were lyophilized overnight and analyzed by MALDI-TOF (see SI).

3. RESULTS AND DISCUSSION

Oligopeptide-decorated Nanomagnets based on Amphiphilic CD.

Synthesis of the nanoassembly components: SC16OH, Ada-Pep and Ada-scPep. SC16OH was synthesized by the conventional procedure[53] with slight modifications in the reaction time and the reactants ratio (see Experimental). The precursor heptakis(6-deoxy-6-hexadecylthio)-β-cyclodextrin was mixed with potassium carbonate, ethylene carbonate and tetramethylurea and heated at 150°C for 5 h, followed by stirring at r.t. for further 16 h. The purified product, heptakis[6-deoxy-6-hexadecylthio-2-poly(ethylene glycol)]-β-cyclodextrin (SC16OH) was characterized by ^{1}H NMR (Figure S2) and ^{13}C NMR (Figure S3). An extensive grafting of the poly(ethyleneglycol) chain (PEG) at the OH-2 was detected by MALDI-TOF-MS (*see below*) and confirmed by the significant peak intensity at 3.65 ppm in the ^{1}H NMR spectrum attributed to the ethylene glycol protons (Figure S2). The extensive oligomerization at the OH-2 was ascribed to the prolonged reaction time for the anionic hydroxyethylation with respect to the reported procedure.[53] The MALDI-TOF mass spectrum of SC16OH consisted of a distribution of peaks centered at about m/z 4216 (Figure 1). The main peaks, detected at m/z 3511+n44, are due to the

presence of molecular species (revealed as MH^+ ions) having different numbers of ethylene oxide (EO) repetitive unit (from 14 to 44) in the PEG arms and corresponding in average to 4-5 units EO per glucose unit (32 EO).

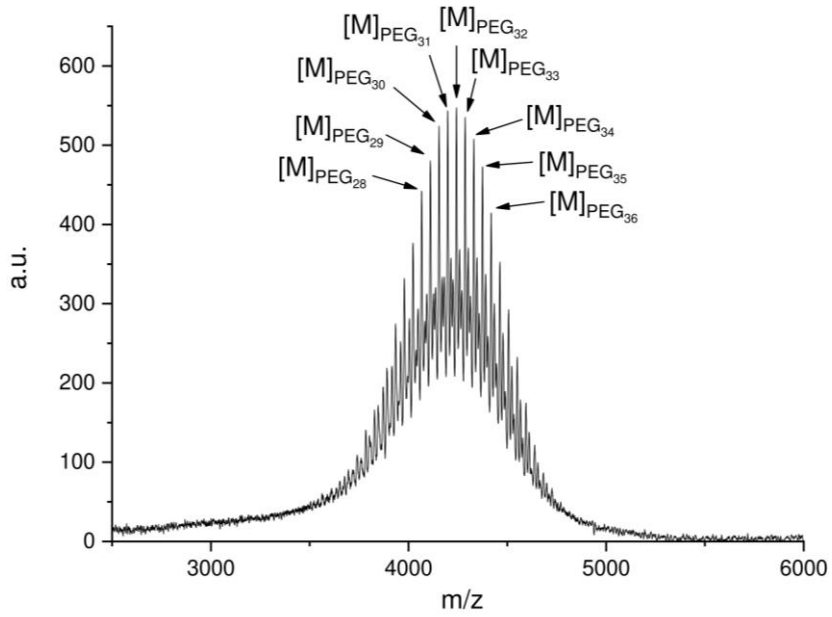

Figure 1. MALDI-TOF mass spectrum of SC16OH. Labels indicate the total number of ethylene oxide repetitive units in PEG arms.

Moreover with the aim to decorate SC16OH, an adamantyl conjugated peptide was synthesized. At this respect, KLVFF peptide was selected due to its ability to recognize the homologous region of the parent full-length Aβ peptide.[27, 29] A $(PEG)_4$ chain, with a similar length as that one functionalizing the secondary rim of SC16OH, was inserted between the pentapeptide and the adamantyl group, exploiting the latter to form inclusion complex with CD cavity.[50,52] Moreover, the scrambled peptide conjugate Ada-*sc*Pep, bearing the VFLKF sequence, was also synthesized to demonstrate the selectivity of KLVFF-decorated nanohybrid towards Aβ (1-42). The peptide conjugates were totally synthesized by using the standard microwave-assisted Solid Phase Peptide Synthesis (mw-SPPS) and their identity was determined by ESI-MS (**Figure S4** and **S5**). Both $(PEG)_4$ and Ada moieties were introduced with the peptide chain still anchored to the solid support.

Preparation and characterization of Nanomagnets based on Amphiphilic CDs (MNP@SC16OH). MNP@SC16OH were prepared by mixing in water pre-formed SC16OH nanovesicles and MNP nanopowder under inert conditions, followed by prolonged stirring at r.t. and subsequent isolation by magnet settling. Similarly to other reported CD functionalised magnetic iron oxide nanocrystals,[65] MNP@SC16OH were obtained by one-step reaction, exploiting the multi-ligand effect of PEG-end hydroxyl groups of the aCD on iron oxide.[66,67] Stabilization on aCD-functionalized MNP was achieved by steric effect of the amphiphile dispersant shell that prevented reversible desorption of capping agent.[68] Interestingly, Ravoo & coworkers designed superparamagnetic NPs (SPIONs), few nanometers sized, embedded in lumen of CD vesicles leading to magnetic field- responsive soft hybrid materials.[69,70] On the other side, our strategy, newly, aimed to get single domain nanomagnets based on an iron oxide core covered with aCD to improve, upon further engineering of the aCD shell, the multifunctionality of the magnetic nano-entity. Accordingly, detection of Aβ was achieved by tailoring MNP@SC16OH nanomagnet with an appropriate KLVFF oligopeptide derivative.

The content of SC16OH on MNP@SC16OH was estimated by TGA under air atmosphere (Figure 2).

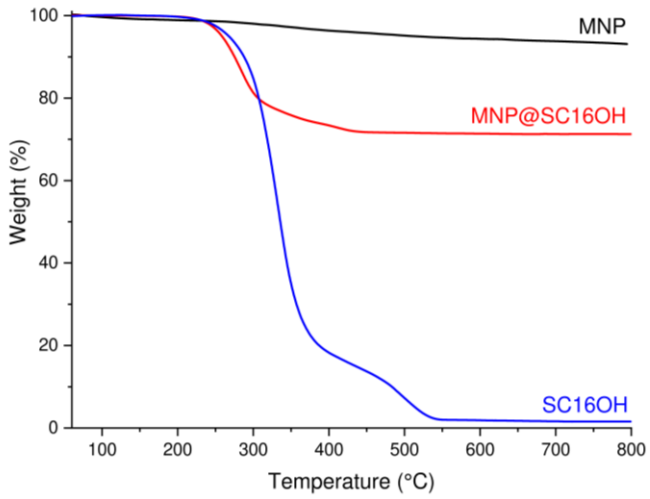

Figure 2. Thermogravimetric profiles of MNP, MNP@SC16OH and SC16OH, in air atmosphere

The TGA profile of MNP revealed a continuous weight loss until 800°C, leaving a residue of about 93%. Instead, the TGA profile of SC16OH showed thermal stability without significant weight loss under 218°C with a double-step decomposition between 218°C and 550°C, with an almost complete decomposition at 800°C. Finally, the thermal profile of MNP@SC16OH showed a decomposition step between 218°C and 450°C, leaving a residue of about 71.1% at 800°C. Based on this result, a SC16OH covering of 21.9 % was calculated.

The XPS surface relative chemical composition of the investigated samples is reported in Table 1. The decrease of the amount of Fe 2p photoelectron signal, along with the detection of carbon and sulphur, on the surface of the MNP@SC16OH clearly demonstrated the interaction between MNP and SC16OH.

Table 1. XPS surface relative chemical composition of the investigated samples. Elemental concentration is expressed as atomic percentage (at. %).

System	C 1s	O 1s	Fe 2p	S 2p
SC16OH	80.0	17.1		2.9
MNP		71.7	28.3	
MNP@SC16OH	75.7	20.2	1.1	3.0

Results of the curve-fitting of Fe $2p_{3/2}$ evidenced the presence of Fe^{2+} and Fe^{3+} ions on the surface of the investigated samples (Figure S6 and Table S1). The component located at BE = 710.0 (where BE is the binding energy) and that at BE = 711.6 eV can be assigned to the presence of iron oxides (Fe_3O_4, FeO) and Fe(OH)O species, respectively. The highest binding energy peak around BE ~ 713.5 eV originated from the peak asymmetry observed in the Fe oxide band envelope.[71-73] A different relative distribution of iron oxy-hydroxides and oxides species was detected on the surface of MNP@SC16OH with respect of that found in MNP. The higher surface Fe(OH)O/FeO ratio (1.5 *vs* 0.3) could be possibly attributed to the interaction between iron hydroxide species on MNP surface and hydroxyls of the SC16OH poly(ethylene glycol) ends. Very similar C 1s spectra were recorded for the pure SC16OH and MNP@SC16OH samples, suggesting a similar surface

distribution of carbon species, both before and after functionalization with MNP. The curve-fitting of C 1s showed a major component located at BE = 285.1 eV assigned to R-C-C and R-C-CH bonds, along with a component at BE = 286.5 eV ascribed to R-C-O and R-C-OH species and a component at BE = 288.4 eV due to the presence of surface R-C-S species (Figure S7 and Table S2). Results of the curve-fitting of O 1s spectra are listed in Table 2 and shown in Figure 3.

Table 2. XPS surface distribution of oxygen species in the investigated samples, resulting from the curve-fitting of O 1s spectra (total peak area = 100%).

BE	**530.5 eV**	**531.3 eV**	**532.7 eV**
Assignment	*Iron Oxides*	*Hydroxides*	*R-C-O, R-C-OH;*
	(Fe_3O_4; FeO)	*$(OH)^-$*	*Fe(OH)O*
SC16OH			100
MNP	82	18	
MNP@SC16OH	17		83

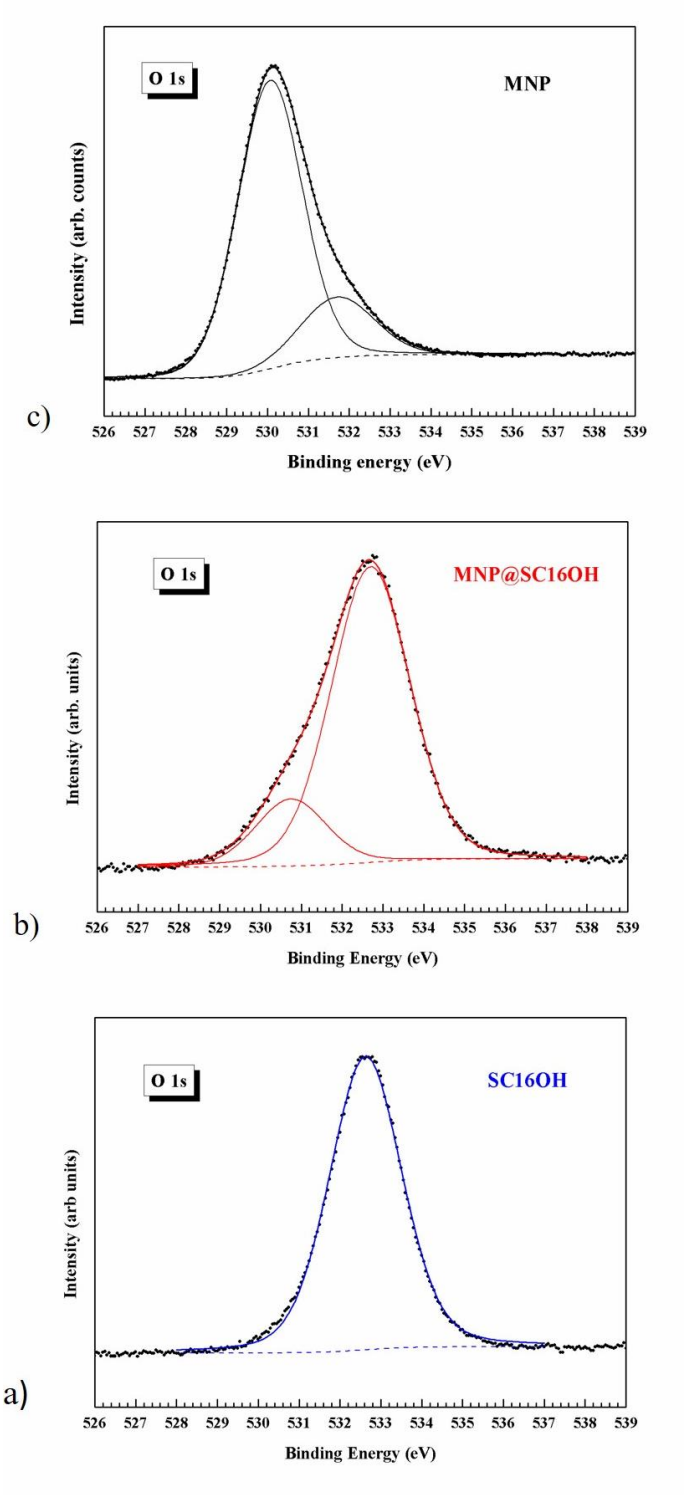

Figure 3. XPS curve-fitting of O 1s spectra in SC16OH (a), MNP (b) and MNP@SC16OH (c).

The O 1s spectrum of SC16OH consisted of a single component located at BE = 532.4 eV that can be assigned to the presence of surface R-C-O; R-C-OH groups.[71] The curve-fitting of O 1s in the MNP@SC16OH sample evidenced a second component at BE = 530.3 eV, which is ascribed to the presence of O^{2-} species in the oxide lattice as in Fe_3O_4.[71] This component is predominant in the curve-fitting of the O 1s peak of the MNP , along with a minor component assigned to hydroxyl groups $(OH)^-$ and Fe(OH)O species (BE = 531.3 eV). The decrease of lattice O^{2-} species on the surface of the aCD-modified MNP with respect of naked MNP strongly agrees with the SC16OH coverage on MNP through a capping process.

The mass magnetization hysteresis loops of pure MNP and of MNP@SC16OH is reported in Figure 4. Both MNP and MNP@SC16OH showed a hysteresis and a coercivity of approximately 95 Oe, which was expected since MNP are ferromagnetic and are not sufficiently small to be superparamagnetic. At an applied field of 1 kOe, MNP@SC16OH owned a reduced mass magnetization (36 emu/g) compared to that of the pure MNP (48 emu/g), likely due to the aCD coating.

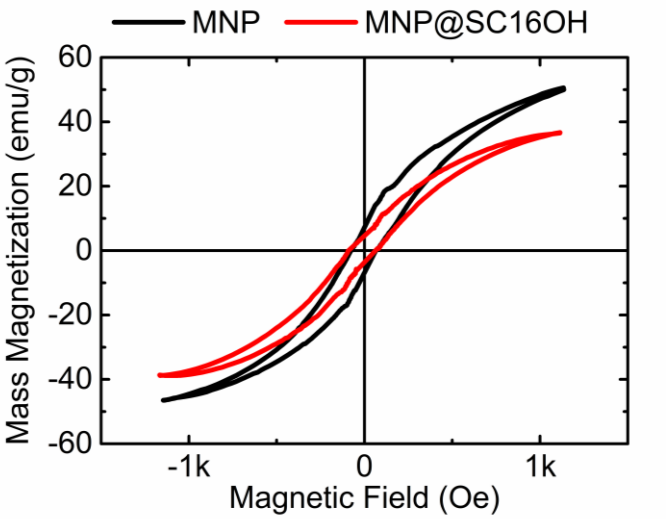

Figure 4. Mass magnetization hysteresis loops of MNP and MNP@SC16OH.

Preparation and characterization of Oligopeptide-decorated aCD Nanomagnets (MNP@SC16OH/Ada-Pep). In search of novel functional nanostructured entities, we envisaged that decorating magnetic iron oxide nanoparticles with aCD bearing an Aβ recognizing peptide

would result in a new hybrid construct able to efficiently interact with Aβ peptides and therefore hampering their self-assembly into oligomeric/fibrillary toxic species. KLVFF-decorated aCD nanomagnets (MNP@SC16OH/Ada-Pep) were prepared by hydration of a KLVFF organic film with the MNP@SC16OH aqueous dispersion and were isolated by two cycles of magnetic settling, centrifugation and washing of the nanoprecipitate. Ada-Pep loading was determined by analysing the supernatant content by MALDI-TOF-MS. The loading was calculated by the difference between the initially added Ada-Pep content and the Ada-Pep amount residual in the supernatant (see Eq 1) which was determined by the linear regression equation of the calibration curve (Figure S1). The amount of Ada-Pep in the supernatant was 15 nmoles ± 5 (17 μg ± 6) and Ada-Pep loading was 362± 5 nmoles (that is 400 ± 6 μg incorporating in 7.6 mg of MNP@SC16OH/Ada-Pep, corresponding to about 54 μg/mg or 48 nmoles/mg of MNP@SC16OH/Ada-Pep) with an entrapment efficiency of about 96 % and an Ada-Pep loading of about 5.3%.

In aqueous dispersion MNP formed sub-micrometer clusters with a hydrodynamic radius (R_H) of about 900 nm and a low electrophoretic mobility of -0.9 micron/s V/cm, corresponding to ζ-potential of about -12 mV. Free SC16OH formed nanoassemblies with R_H of about 100 nm and ζ-potential of about -40 mV. MNP was stabilized by the covering effect of SC16OH yielding MNP@SC6OH nanoclusters with a R_H of about 150 nm and an enhanced (more negative) electrophoretic mobility of -3.16 μm/s V/cm corresponding to a ζ-potential of -35 mV (Figure 5 and Table 3). MNP@SC6OH/Ada-Pep showed similar R_H *vs* MNP@SC16OH and a lower ζ-potential (-30 mV), indicating stability of KLVFF-tailored nanomagnet in aqueous dispersion, without precipitation. This decrease of ζ-potential can be ascribed to the partial neutralization of the surface charge after entanglement of Ada-Pep in MNP@SC16OH, as observed for non-magnetic SC16OH/Ada-Pep showing a positive electrophoretic mobility of 2.2 μm/s V/cm (*data not shown*).

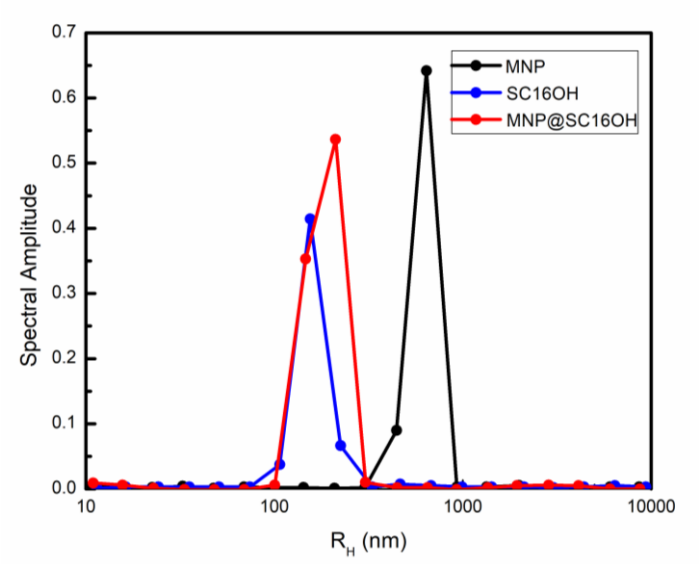

Figure 5. Size distribution of MNP, SC16OH and MNP@SC16OH.

Table 3: Hydrodynamic Radius (R_H), polydispersity index (PI), electrophoretic mobility (μ) and ζ-potential of aCD-based nanomagnets (MNP@SC16OH and MNP@SC16OH/Ada-Pep) *vs* SC16OH and MNP.

System	R_H (nm)	PI	μ (μm/sV/cm)	ζ-potential (mV)
MNP	900	0.30	-0.9	-12
SC16OH	100	0.30	-3	-40
MNP@SC16OH	150	0.30	-3.16	-35
MNP@SC16OH/Ada-Pep	150	0.40	-2.4	-30

Morphology of aCD-decorated nanomagnets are reported in Figure 6. TEM images of MNP@SC16OH/Ada-Pep (Figure 6 A-C) showed single domain nanoassemblies with size of

about 30-50 nm in which single MNP capped by SC16OH bi- or multilayers were clearly observed, analogously to other metal NPs covered with aCD functionalized with long-thioalkyl chain.[47] The incorporation of magnetic entities in oligopeptide-modified aCD nanovescicles was demonstrated by respective diffraction pattern (Figure 6D) and STEM of MNP@SC16OH/Ada-Pep (Figure 6E, *i-vi*) that semi-quantitatively evidenced the presence of the peculiar elements belonging both to MNP (iron and oxygen) and SC16OH/Ada-Pep (carbon, oxygen, sulfur, nitrogen).

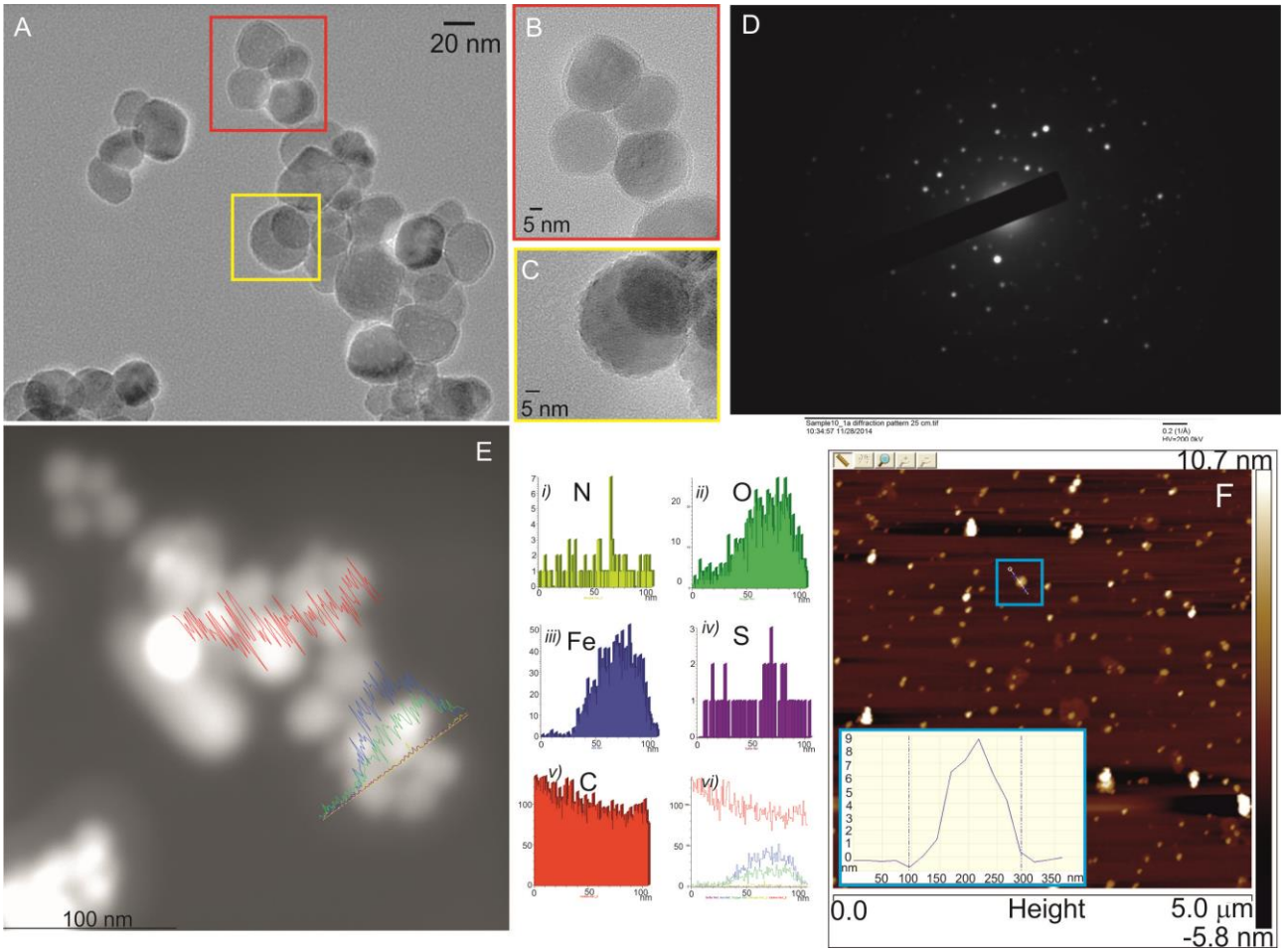

Figure 6. Representative TEM images of MNP@SC16OH/Ada-Pep at low (A) and high resolution (B,C) with diffraction pattern on nanoassembly clusters shown in A (D). STEM of MNP@SC16OH/Ada-Pep with linescans displaying total elemental analysis taken at 100 nm scale length (E), detected by peculiar emission lines of elements (*i*–*v*) and total elemental analysis percentage (*vi*). Representative AFM image of MNP@SC16OH/Ada-Pep collected on 5 µm x 5µm with enlarged profile (taken at 200 nm scale length) showing a nanomagnet about 50 nm wide and 9 nm high.

TEM micrographs exhibited clusters of nanoassemblies with sizes higher than 100 nm, in agreement with DLS results. Moreover, AFM microscopy carried out on samples casted on mica surface showed the presence of clusters with the size ranging 50-200 nm and about 10 nm high (Figure 6F).

Molecular fishing of Aβ (1-42) by KLVFF Oligopeptide-Decorated aCD Nanomagnets.

In view of a suitable application of our magnetic nanoconstructs as diagnostic tools, we investigated the ability of MNP@SC16OH/Ada-Pep to capture Aβ (1-42) protein in aqueous medium. Our aim was to demonstrate that KLVFF -decorated aCD nanomagnets captured Aβ (1-42) by MALDI-TOF-MS detection following an optimized fishing protocol (**Figure 7**).

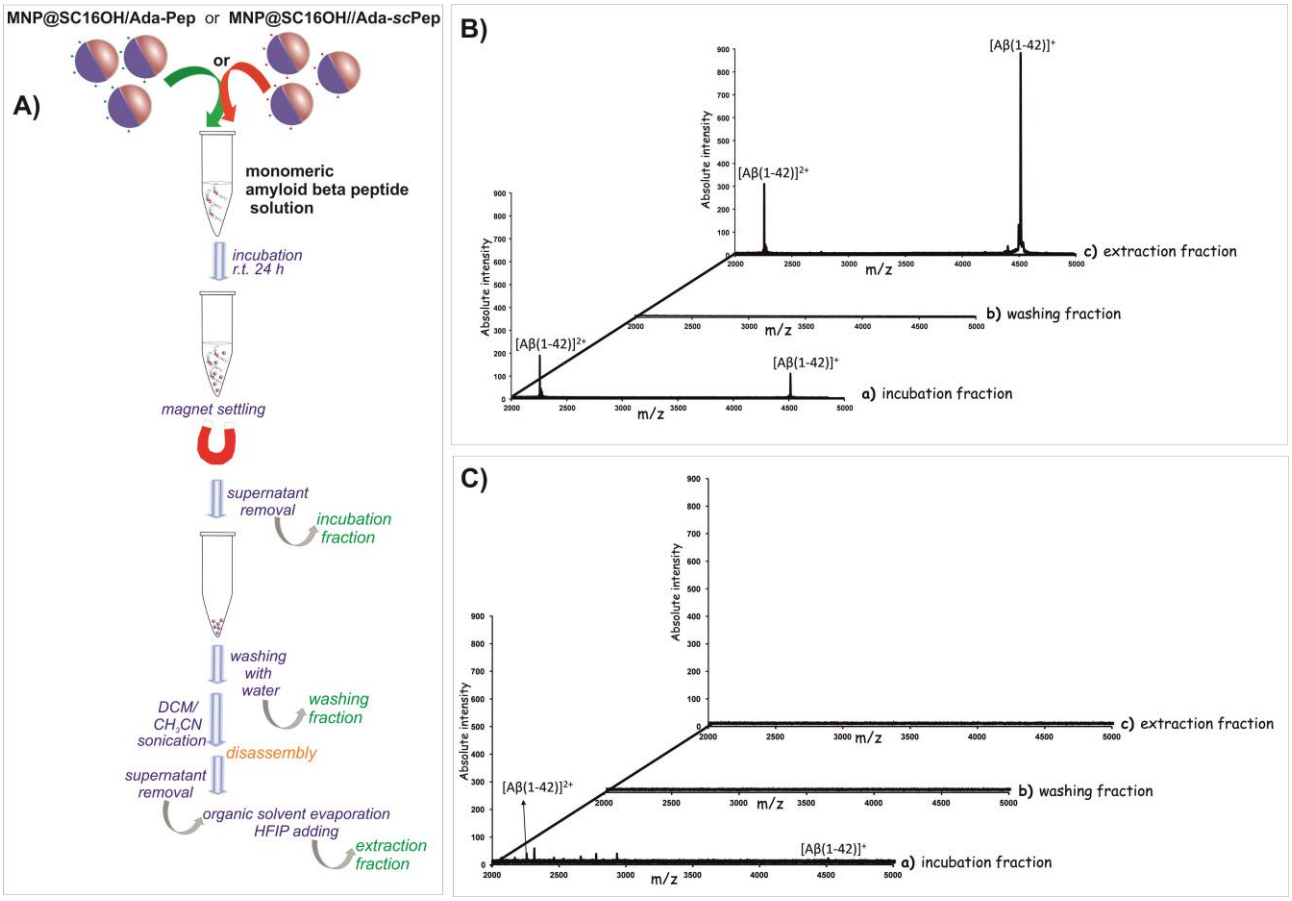

Figure 7. Main steps of the optimized fishing protocol (A, see experimental); MALDI-TOF-MS acquired after Aβ (1-42) fishing with MNP@SC16OH/Ada-Pep (B) and MNP@SC16OH/*sc*Ada-Pep (C). The mass

measurements were performed in a) supernatant solution after incubation of Aβ (1-42) aqueous sample with the nanomagnets (incubation fraction); b) water solution used for washing nanomagnets after incubation process (washing fraction); c) DCM/CH_3CN (97/3) used to disrupt the interactions between the Aβ (1-42) peptide and the Ada-Pep immobilized in the nanomagnets (extraction fractions). Before MALDI-TOF-MS, all the samples (incubation fraction, washing fraction and extraction fraction) were frozen at −30 °C and the iced solutions were lyophilized overnight.

Three different fractions were obtained after co-incubation of KLVFF-decorated nanomagnets with Aβ (1-42) solutions (see Figure 7B) and all the collected fractions were analysed by MALDI-TOF-MS. In particular, the MALDI-TOF mass spectrum of the incubation fraction (Figure 7B, trace a) show two signals at m/z 4514 and 2257, corresponding to the mono and double charge of Aβ (1-42) respectively. The observed Aβ (1-42) signals indicated the excess of amyloid not retained by nanomagnets that was completely removed by rinsing out the NPs with milli Q water as evidenced in Figure 7B, trace b. Finally, the addition of a mixture of organic solvents (DCM/CH_3CN, 97/3) aided the disassembly of the nanoconstruct by extracting both bonded Aβ (1-42) from peptide and Ada-Pep immobilized in the nanomagnets (extraction fraction, trace c). Interestingly, the MALDI-TOF mass spectrum reported in Figure 7B, trace c revealed a high-intensity m/z signals corresponding to the Aβ (1-42) suggesting that most of peptide was retained by MNP@SC16OH/Ada-Pep. Therefore, the comparison of the spectra reported in Figure 7B (traces a-c) suggested that KLVFF-decorated MNP@SC16OH were able to interact with Aβ (1-42) monomer catching it out from the aqueous solution.

To reduce signal variability, mass spectra acquired for each fraction (15 spectra, see experimental) were averaged and monoisotopic peaks were automatically picked up. Spectra are reported in absolute values in Figure 7B and used to semi-quantatively estimate Aβ (1-42). Despite the low reproducibility of MALDI measurements, the averaged values of Aβ (1-42) signal intensity recorded over 15 replicate measurements, revealed a reasonable homogenity between the amount of Aβ (1-42) and the corresponding signal intensities. This was supported by the calibration curve calculated from MALDI-TOF averaged spectra of Ada-Pep standard (see Figure S1 in SI).

The results of crucial experiments demonstrating the selectivity of our nanomagnet are reported in Figure S8 and 7C: undecorated MNP@SC16OH and MNP@SC16OH/Ada-*sc*Pep nanomagnets were used to operate Aβ (1-42) fishing under thye same experimental conditions.

It is clear from Figure S8, that the incubation fraction (trace a) exhibits very low intensity signal correspond to unbound Aβ (1-42) monomers. This is even more evident if compared with the corresponding MALDI-TOF mass spectrum reported in Figure 7B (trace a). It is worth noting that the MALDI-TOF-MS were acquired after 24h of incubation of the Aβ (1-42) solution with the nanomagnets. The low intensity of the Aβ (1-42) peak observed in Figure S8 (trace a) is ascribable to an extensive peptide aggregation that occurred during the incubation time. By contrast, when MNP@SC16OH/Ada-Pep were used, the Aβ (1-42) aggregation was significantly slowed down because of the presence of the KLVFF that is known to stabilize the monomeric form of Aβ 1-42 avoiding its recruitment into aggregate forms.[74]

Interestingly, the Aβ (1-42) fishing experiments performed with the scrambled peptide-decorated MNP@SC16OH/Ada-*sc*Pep nanomagnet confirmed the sequence-specific recognition ability of the native KLVFF sequence. Moreover, the absence of m/z signals corresponding to Aβ (1-42) in MALDI-TOF-MS reported in Figure 7C indicated that the scrambled analogue was neither able to recruit Aβ(1-42) from incubation solution nor to prevent Aβ (1-42) aggregation.

A hypothesized arrangement of the capture of Aβ (1-42) by KLVFF-decorated aCD nanomagnets was proposed in Scheme 1. The interaction of Aβ (1-42) on the surface of nanomagnets was likely driven by the self-recognition between KLVFF regions belonging to Aβ (1-42) and the homologous peptide sequence exposed on the surface of aCD capped nanomagnets, through H-bonding and hydrophobic interactions in well agreement with previous reports.[27-29] This hypothesis was further proved by the ineffectiveness of MNP@SC16OH/Ada-*sc*Pep to recruit Aβ (1-42), as no selective interactions between β-sheets of scrambled oligopeptide (VFLKF) on nanomagnets surface and Aβ(1-42) sequence could take place.

Altogether, the results reported in this study point out the key role of the KLVFF peptide in endowing the nanomagnets with specific recognition of the Aβ (1-42). The comparative analysis with nanomagnets decorated with the scrambled peptide further validate this result. The ability of the designed nanoconstruct to selectively detect the amyloid peptides in sample solutions containing other peptides/proteins still remains to be explored. The effectiveness of these potential diagnostic tools might be proved by setting up experiments with artificial mixtures, as first attempt, followed by validation with biological fluids. In this regards studies are in progress in our labs.

4. CONCLUSIONS

We have proposed novel nanomagnets based on amphiphilic cyclodextrin (SC16OH) decorated with a KLVFF oligopeptide prepared by a green capping reaction in aqueous solution for the selective recognition and capture of Aβ (1-42). SC16OH bi- or multilayers covered magnetic nanoparticles forming single domain nanomagnets of about 30-50 nm. Adamantyl-conjugate of KLVFF was incorporated in MNP@SC16OH thanks to the high binding affinity between adamantane and CD cavity, together with entanglement interactions between PEG arms of similar length to polyethylene glycol chain on the secondary rim of CD. MNP@SC16OH exhibited a reduced mass magnetization compared to that of the pure MNP, plausibly due to the amphiphilic CD coating. In aqueous dispersion MNP micrometric aggregates were stabilized by the covering effect of SC16OH, forming MNP@SC6OH nanoclusters with R_H of about 150 nm and a negative zeta potential (-35 mV) which became less negative (-30 mV) after incorporation of Ada-Pep, assessing the exposition of KLVFF on nanomagnet surface. Finally, our nanomagnets incorporating about 50 nmoles of Ada-Pep per mg of MNP@SC6OH/Ada-Pep were able to selectively recognize and capture Aβ (1-42) in aqueous solution whereas not decorated nanomagnets or scrambled peptide (VFLKF)-decorated ones were not able to recruit amyloid peptide. In perspective, these nanomagnets coupled with the highly sensitive MALDI-TOF detection could pave the way to straight applications in fishing amyloids from fluids of Alzheimer patients by magnetic manipulation of small volumes of aqueous media, thus speeding up the diagnostic response.

ACKNOWLEDGMENT

The authors thank PON02_00665 (02_00355_2964193 HYPPOCRATES) and CNR (Project ISMN-CNR: Materials and Dispositives for Health and Life Quality) for financial support

Supporting Information: Methods: Mass Spectrometry; X-Ray Photoelectron Spectroscopy XPS; Detection by MALDI-TOF-MS following fishing protocol. Figures: Calibration curve for Ada-Pep by MALDI–TOF-MS (Figure S1); ^{1}H NMR of SC16OH (Figure S2); ^{13}C NMR of SC16OH (Figure S3); ESI-MS of Ada-Pep (Figure S4); ESI-MS of Ada-*sc*Pep (Figure S5); XPS

curve-fitting of Fe $2p_{3/2}$ spectra of MNP and MNP@SC16OH (Fugure S6); XPS surface distribution of Iron species in MNP and MNP@SC16OH (Table S1); XPS curve-fitting of the C 1s spectrum in SC16OH and MNP@SC16OH (Figure S7); XPS surface distribution of Carbon species in in SC16OH and MNP@SC16OH (Table S2); MALDI-TOF-MS acquired after Aβ 1-42 fishing with MNP@SC16OH (Figure S8).

Corresponding Authors

*Antonino Mazzaglia, Consiglio Nazionale delle Ricerche, Istituto per lo Studio dei Materiali Nanostrutturati (CNR-ISMN), Viale F. Stagno D'Alcontres 31, Messina 98166, Italy

Email: antonino.mazzaglia@cnr.it

*Norberto Micali, Consiglio Nazionale delle Ricerche, Istituto per i Processi Chimico-Fisici (CNR-IPCF), Viale Ferdinando Stagno d'Alcontres 37, 98158 Messina

Email: norberto.micali@cnr.it

* Giuseppe Pappalardo, Consiglio Nazionale delle Ricerche, Istituto di Cristallografia (CNR-IC), Via P. Gaifami 18, 95126 Catania, Italy

Email: giuseppe.pappalardo@cnr.it

Author Contributions

The manuscript was written through the contributions of all authors. All authors have given approval to the final version of the manuscript.

REFERENCES

1 Revia, R. A.; Zhang, M. Magnetite nanoparticles for cancer diagnosis, treatment, and treatment monitoring: recent advances. *Materials Today* **2016**, *19* (3), 157-168. http://dx.doi.org/10.1016/ j.mattod.2015.08.022.

2 Carvalho, C. L. C.; Silva, A. T. B.; Luz, R. A. S.; Castro, G. M. B.; Lima, C. da L.; Mastelaro, V. R.; da Silva, R. R.; Osvaldo N. Oliveira, Jr.; Cantanhêde, W. Development of $Co_3[Co(CN)_6]_2/Fe_3O_4$ Bifunctional Nanocomposite for Clinical Sensor Applications. *ACS Applied Nano Materials* **2018**, *1* (8), 4283–4293. https://doi.org/10.1021/ACSANM.8B01106.

3 Du, Z.; Gao, N.; Guan, Y.; Ding, C.; Sun, Y.; Ren, J.; Qu, X. Rational Design of a "Sense and Treat" System to Target Amyloid Aggregates Related to Alzheimer's Disease. *Nano Res.* **2018**, *11* (4), 1987–1997. https://doi.org/10.1007/s12274-017-1815-9.

4 Rivas, J.; Bañobre-López, M.; Piñeiro-Redondo, Y.; Rivas, B.; López-Quintela, M. A. Magnetic Nanoparticles for Application in Cancer Therapy. *Journal of Magnetism and Magnetic Materials* **2012**, *324* (21), 3499–3502. https://doi.org/10.1016/j.jmmm.2012.02.075.

5 Farzin, A.; Etesami, S. A.; Quint, J.; Memic, A.; Tamayol, A. Magnetic Nanoparticles in Cancer Therapy and Diagnosis. *Advanced Healthcare Materials* **2020**, *9* (9), 1901058. https://doi.org/10.1002/adhm.201901058.

6 Ulbrich, K.; Holá, K.; Šubr, V.; Bakandritsos, A.; Tuček, J.; Zbořil, R. Targeted Drug Delivery with Polymers and Magnetic Nanoparticles: Covalent and Noncovalent Approaches, Release Control, and Clinical Studies. *Chemical reviews* **2016,** *116* (9), 5338-5431. https://doi.org/10.1021/acs.chemrev.5b00589.

7 Skorjanc, T.; Benyettou, F.; Olsen, J.-C.; Trabolsi, A. Design of Organic Macrocycle-Modified Iron Oxide Nanoparticles for Drug Delivery. *Chemistry – A European Journal* **2017**, *23* (35), 8333–8347. https://doi.org/10.1002/chem.201605246.

8 Meikle, S. T.; Piñeiro, Y.; Bañobre López, M.; Rivas, J.; Santin, M. Surface functionalization superparamagnetic nanoparticles conjugated with thermoresponsive poly(epsilon-lysine) dendrons tethered with carboxybetaine for the mild hyperthermia-controlled delivery of VEGF, *Acta Biomaterialia*, **2016**, *40*, 235-242 https://doi.org/10.1016/j.actbio.2016.04.043.

9 Jeon, H.; Kim, J.; Lee, Y. M.; Kim, J.; Choi, H. W.; Lee, J.; Park, H.; Kang, Y.; Kim, I.-S.; Lee, B.-H.; Hoffman, A. S.; Kim, W. J. Poly-Paclitaxel/Cyclodextrin-SPION Nano-Assembly for Magnetically Guided Drug Delivery System. *J Control Release* **2016**, *231*, 68–76. https://doi.org/10.1016/j.jconrel.2016.01.006.

10 Cha, R.; Li, J.; Liu, Y.; Zhang, Y.; Xie, Q.; Zhang, M. Fe_3O_4 Nanoparticles Modified by CD-Containing Star Polymer for MRI and Drug Delivery. *Colloids and Surfaces B: Biointerfaces* **2017**, *158*, 213–221. https://doi.org/10.1016/j.colsurfb.2017.06.049.

11 Fan, C.-Y.; Hou, Y.-R.; K. Adak, A.; T. Waniwan, J.; Rosa, M. A. C. dela; Yeir Low, P.; Angata, T.; Hwang, K.-C.; Chen, Y.-J.; Lin, C.-C. Boronate Affinity-Based Photoactivatable Magnetic Nanoparticles for the Oriented and Irreversible Conjugation of Fc-Fused Lectins and Antibodies. *Chem. Sci.* **2019**, *10* (37), 8600–8609. https://doi.org/10.1039/c9sc01613a.

12 Ashrafian, H.; Zadeh, E. H.; Khan, R. H. Review on Alzheimer's Disease: Inhibition of Amyloid Beta and Tau Tangle Formation. *International Journal of Biological Macromolecules* **2021**, *167*, 382–394. https://doi.org/10.1016/j.ijbiomac.2020.11.192.

13 Baldassarre, M.; Baronio, C. M.; Morozova-Roche, L. A.; Barth, A. Amyloid β-Peptides 1–40 and 1–42 Form Oligomers with Mixed β-Sheets. *Chem. Sci.* **2017**, *8* (12), 8247–8254. https://doi.org/10.1039/c7sc01743j.

14 Gu, L.; Guo, Z. Alzheimer's Aβ42 and Aβ40 Peptides Form Interlaced Amyloid Fibrils. *J Neurochem* **2013**, *126* (3), 305–311. https://doi.org/10.1111/jnc.12202.

15 Giacomelli, C.; Daniele, S.; Martini, C. Potential biomarkers and novel pharmacological targets in protein aggregation-related neurodegenerative diseases. *Biochem. Pharmacol.* **2017**, *131*, 1-15. https://doi.org/10.1016/j.bcp.2017.01.017.

16 Van Thanh Nguyen, N.; Taverna, M.; Smadja, C.; Thanh Duc Mai T. D. Recent Electrokinetic and Microfluidic Strategies for Detection of Amyloid Beta Peptide Biomarkers: Towards Molecular Diagnosis of Alzheimers Disease *Chem. Rec.* **2020**, *20*, 1–14. https://doi.org/10.1002/tcr.202000103.

17 Stefan-van Staden, R.-I.; Popa-Tudor, I.; Badulescu, M.; Anghel, A. Fast Screening Method for Molecular Recognition of Islet Amyloid Polypeptide from Whole Blood Samples Collected from Diabetic Patients with Disposable Stochastic Sensors Obtained by Nanolayer, and Nanolayer by Nanolayer Deposition Using Cold Plasma. *Anal Bioanal Chem* **2020**, *412* (17), 4135–4141. https://doi.org/10.1007/s00216-020-02646-0.

18 Liu, B.; Shen, H.; Hao, Y.; Zhu, X.; Li, S.; Huang, Y.; Qu, P.; Xu, M. Lanthanide Functionalized Metal-Organic Coordination Polymer: Toward Novel Turn-On Fluorescent Sensing of Amyloid β-Peptide. *Anal Chem* **2018**, *90* (21), 12449–12455. https://doi.org/10.1021/acs.analchem.8b01546.

19 Pansieri, J.; Gerstenmayer, M.; Lux, F.; Mériaux, S.; Tillement, O.; Forge, V.; Larrat, B.; Marquette, C. Magnetic Nanoparticles Applications for Amyloidosis Study and Detection: A Review. *Nanomaterials* **2018**, *8* (9), 740. https://doi.org/10.3390/nano8090740.

20 Li, Y.; Lim, E.; Fields, T.; Wu, H.; Xu, Y.; Wang, Y. A.; Mao, H. Improving Sensitivity and Specificity of Amyloid-β Peptides and Tau Protein Detection with Antibiofouling Magnetic Nanoparticles for Liquid Biopsy of Alzheimer's Disease. *ACS Biomater. Sci. Eng.* **2019**, *5* (7), 3595–3605. https://doi.org/10.1021/acsbiomaterials.9b00086.

21 Du, Z.; Gao, N.; Guan, Y.; Ding, C.; Sun, Y.; Ren, J.; Qu, X. Rational design of a "sense and treat" system to target amyloid aggregates related to Alzheimer's disease. *Nano Research* 2018, 11(4): 1987–1997. https://doi.org/10.1007/s12274-017-1815-9

22 Pi, J.; Long, Y.; Huang, N.; Cheng, Y.; Zheng, H. A Sandwich Immunoassay for Detection of Aβ1-42 Based on Quantum Dots. *Talanta* **2016**, *146*, 10–15. https://doi.org/10.1016/j.talanta.2015.08.022.

23 Jiang, L.-F.; Chen, B.-C.; Chen, B.; Li, X.-J.; Liao, H.-L.; Huang, H.-M.; Guo, Z.-J.; Zhang, W.-Y.; Wu, L. Detection of Aβ Oligomers Based on Magnetic-Field-Assisted Separation of Aptamer-Functionalized Fe3O4 Magnetic Nanoparticles and BaYF5:Yb,Er Nanoparticles as Upconversion Fluorescence Labels. *Talanta* **2017**, *170*, 350–357. https://doi.org/10.1016/j.talanta.2017.04.021.

24 Hassan, N.; L. Cordero, M.; Sierpe, R.; Almada, M.; Juárez, J.; Valdez, M.; Riveros, A.; Vargas, E.; Abou-Hassan, A.; M. Ruso, J.; J. Kogan, M. Peptide Functionalized Magneto-Plasmonic Nanoparticles Obtained by Microfluidics for Inhibition of β-Amyloid Aggregation. *Journal of Materials Chemistry B* **2018**, *6* (31), 5091–5099. https://doi.org/10.1039/C8TB00206A.

25 Kim, D.; Kwon, H. J.; Hyeon, T. Magnetite/Ceria Nanoparticle Assemblies for Extracorporeal Cleansing of Amyloid-β in Alzheimer's Disease. *Advanced Materials* **2019**, *31* (19), 1807965. https://doi.org/10.1002/adma.201807965.

26 De la Torre, C.; Ceña, V. The Delivery Challenge in Neurodegenerative Disorders: The Nanoparticles Role in Alzheimer's Disease Therapeutics and Diagnostics. *Pharmaceutics* **2018**, *10* (4), 190. https://doi.org/10.3390/pharmaceutics10040190.

27 Tjernberg, L. O.; Lilliehöök, C.; Callaway, D. J. E.; Näslund, J.; Hahne, S.; Thyberg, J.; Terenius, L.; Nordstedt, C. Controlling Amyloid β-Peptide Fibril Formation with Protease-Stable Ligands. *Journal of Biological Chemistry* **1997**, *272* (19), 12601–12605. https://doi.org/10.1074/jbc.272.19.12601.

28 Yang, P.; Yang, C.; Zhang, K.; Wang, L.; Wang, H. KLVFF Peptide Functionalized Nanoparticles Capture Aβ42 by Co-Assembly for Decreasing Cytotoxicity. *Chinese Chemical Letters* **2018**, *29* (12), 1811–1814. https://doi.org/10.1016/j.cclet.2018.10.003.

29 Chafekar, S. M.; Malda, H.; Merkx, M.; Meijer, E. W.; Viertl, D.; Lashuel, H. A.; Baas, F.; Scheper, W. Branched KLVFF Tetramers Strongly Potentiate Inhibition of Beta-Amyloid Aggregation. *ChemBioChem* **2007**, *8* (15), 1857–1864. https://doi.org/10.1002/cbic.200700338.

30 Goyal, D.; Shuaib, S.; Mann, S.; Goyal, B.; Rationally designed peptides and Peptidomimetics as inhibitors of Amyloid-β (Aβ) aggregation: potential therapeutics of alzheimer's disease. *ACS Comb. Sci.* **2017**, *19*, 55–80. https://doi.org/10.1021/ acscombsci.6b00116.

31 Skaat, H.; Shafir, G.; Margel, S. Acceleration and Inhibition of Amyloid-β Fibril Formation by Peptide-Conjugated Fluorescent-Maghemite Nanoparticles. *J Nanopart Res* **2011**, *13* (8), 3521–3534. https://doi.org/10.1007/s11051-011-0276-4.

32 Plissonneau, M.; Pansieri, J.; Heinrich-Balard, L.; Morfin, J.-F.; Stransky-Heilkron, N.; Rivory, P.; Mowat, P.; Dumoulin, M.; Cohen, R.; Allémann, É.; Tóth, É.; Saraiva, M. J.; Louis, C.; Tillement, O.; Forge, V.; Lux, F.; Marquette, C. Gd-Nanoparticles Functionalization with Specific Peptides for ß-Amyloid Plaques Targeting. *J Nanobiotechnol* **2016**, *14* (1), 60. https://doi.org/10.1186/s12951-016-0212-y.

33 Fourmentin, S.; Crini, G.; Lichtfouse, E. *Cyclodextrin Fundamentals, Reactivity and Analysis*; 2018, Springer International Publishing, Springer Nature Switzerland AG. https://doi.org/10.1007/978-3-319-76159-6.

34 Xia, N.; Wang, X.; Zhou, B.; Wu, Y.; Mao, W.; Liu, L. Electrochemical Detection of Amyloid-β Oligomers Based on the Signal Amplification of a Network of Silver Nanoparticles. *ACS Appl. Mater. Interfaces* **2016**, *8* (30), 19303–19311. https://doi.org/10.1021/acsami.6b05423.

35 Bhasikuttan, A. C.; Mohanty, J. Detection, Inhibition and Disintegration of Amyloid Fibrils: The Role of Optical Probes and Macrocyclic Receptors. *Chem Commun (Camb)* **2017**, *53* (19), 2789–2809. https://doi.org/10.1039/c6cc08727b.

36 Li, X.; Li, J.; Liu, Y.; Zhang, X.; Chen, J. A Sensitive Electrochemical Immunosensor for Prion Detection Based on Poly-β-Cyclodextrin/Gold Nanoparticles/Glassy Carbon Electrode. *Sensors and Actuators B: Chemical* **2017**, *250*, 1–7. https://doi.org/10.1016/j.snb.2017.04.101.

37 Moreira, F. T. C.; Sales, M. G. F. Smart Naturally Plastic Antibody Based on Poly(α-Cyclodextrin) Polymer for β-Amyloid-42 Soluble Oligomer Detection. *Sensors and Actuators B: Chemical* **2017**, *240*, 229–238. https://doi.org/10.1016/j.snb.2016.08.150.

38 Duan, S.; Li, J.; Zhao, N.; Xu, F.-J. Multifunctional Hybrids with Versatile Types of Nanoparticles via Self-Assembly for Complementary Tumor Therapy. *Nanoscale* **2018**, *10* (16), 7649–7657. https://doi.org/10.1039/c8nr00767e.

39 Mrówczyński, R.; Jędrzak, A.; Szutkowski, K.; Grześkowiak, B. F.; Coy, E.; Markiewicz, R.; Jesionowski, T.; Jurga, S. Cyclodextrin-Based Magnetic Nanoparticles for Cancer Therapy. *Nanomaterials* **2018**, *8* (3), 170. https://doi.org/10.3390/nano8030170.

40 Chen, P.; Song, H.; Yao, S.; Tu, X.; Su, M.; Zhou L. Magnetic Targeted Nanoparticles based on β-Cyclodextrin and Chitosan for Hydrophobic Drug Delivery and a Study of their Mechanism. *RSC Adv*., **2017**, *7*, 29025-29034. https://doi.org/10.1039/c7ra02398g.

41 Peng, L.; Luo, Y.; Xiong, H.; Yao, S.; Zhu, M.; Song, H. A Novel Amperometric Glucose Biosensor Based on Fe_3O_4-Chitosan-β-Cyclodextrin/MWCNTs Nanobiocomposite. *Electroanalysis* **2020**, *32*, 1–11. https://doi.org/10.1002/elan.202060399.

42 Muñoz, J.; Crivillers, N.; Ravoo, B. J.; Mas-Torrent, M. Cyclodextrin-Based Superparamagnetic Host Vesicles as Ultrasensitive Nanobiocarriers for Electrosensing. *Nanoscale* **2020**, *12*, 9884-9889. https://doi.org/10.1039/d0nr01702g.

43 Ansari, M.; Habibi-Rezaei, M; Salahshour-Kordestani, S.; Ferdousi, M.; Moosavi-Movahedi, A.A. An Investigation on the Effect of β-CD Modified Fe_3O_4 Magnetic Nanoparticles on Aggregation of Amyloid β Peptide (25-35). *Materials Technology* **2016**, *31*(6), 315-321. https://doi.org/10.1179/17535557B15Y.000000002.

44 Mazzaglia, A.; Scala, A.; Sortino, G.; Zagami, R.; Zhu, Y.; Sciortino, M. T.; Pennisi, R.; Pizzo, M. M.; Neri, G.; Grassi, G.; Piperno, A. Intracellular Trafficking and Therapeutic Outcome of Multiwalled Carbon Nanotubes Modified with Cyclodextrins and Polyethylenimine. *Colloids and Surfaces B: Biointerfaces* **2018**, *163*, 55–63. https://doi.org/10.1016/j.colsurfb.2017.12.028.

45 Piperno, A.; Mazzaglia, A.; Scala, A.; Pennisi, R.; Zagami, R.; Neri, G.; Torcasio, S. M.; Rosmini, C.; Mineo, P. G.; Potara, M.; Focsan, M.; Astilean, S.; Zhou, G. G.; Sciortino, M. T. Casting Light on Intracellular Tracking of a New Functional Graphene-Based MicroRNA Delivery System by FLIM and Raman Imaging. *ACS Appl Mater Interfaces* **2019**, *11* (49), 46101–46111. https://doi.org/10.1021/acsami.9b15826.

46 Neri, G.; Cordaro, A.; Scala, A.; Cordaro, M.; Mazzaglia, A.; Piperno, A. PEGylated Bis-Adamantane Carboxamide as Guest Bridge for Graphene Poly-Cyclodextrin Gold Nanoassemblies. *Journal of Molecular Structure* **2021**, *1240*, 130519. https://doi.org/10.1016/j.molstruc.2021.130519.

47 Trapani, M.; Scala, A.; Mineo, P. G.; Pistone, A.; Díaz-Moscoso, A.; Fragoso, A.; Monsù Scolaro, L.; Mazzaglia, A. Thiolated Amphiphilic β-Cyclodextrin-Decorated Gold Colloids: Synthesis, Supramolecular Nanoassemblies and Controlled Release of Dopamine. *Journal of Molecular Liquids* **2021**, *336*, 116880. https://doi.org/10.1016/j.molliq.2021.116880.

48 Trapani, M.; Romeo, A.; Parisi, T.; Sciortino, M. T.; Patané, S.; Villari, V.; Mazzaglia, A. Supramolecular Hybrid Assemblies Based on Gold Nanoparticles, Amphiphilic Cyclodextrin and Porphyrins with Combined Phototherapeutic Action. *RSC Adv*., **2013**, *3*, 5607–5614. https://doi.org/10.1039/c3ra40204e.

49 Xu, Z.; Jia, S.; Wang, W.; Yuan, Z.; Ravoo, B. J.; Guo, D.-S. Heteromultivalent Peptide Recognition by Co-Assembly of Cyclodextrin and Calixarene Amphiphiles Enables Inhibition of Amyloid Fibrillation. *Nature Chem* **2019**, *11* (1), 86–93. https://doi.org/10.1038/s41557-018-0164-y.

50 Zagami, R.; Rapozzi, V.; Piperno, A.; Scala, A.; Triolo, C.; Trapani, M.; Xodo, L. E.; Monsù Scolaro, L.; Mazzaglia, A. Folate-Decorated Amphiphilic Cyclodextrins as Cell-Targeted Nanophototherapeutics. *Biomacromolecules* **2019**, *20* (7), 2530–2544. https://doi.org/10.1021/acs.biomac.9b00306.

51 Cordaro, A.; Zagami, R.; Malanga, M.; Venkatesan, J. K.; Alvarez-Lorenzo, C.; Cucchiarini, M.; Piperno, A.; Mazzaglia, A. Cyclodextrin Cationic Polymer-Based Nanoassemblies to Manage Inflammation by Intra-Articular Delivery Strategies. *Nanomaterials* **2020**, *10* (9), 1712. https://doi.org/10.3390/nano10091712.

52 Viale, M.; Tosto, R.; Giglio, V.; Pappalardo, G.; Oliveri, V.; Marić, I.; Mariggiò, M.; Vecchio, G. Cyclodextrin Polymers Decorated with RGD Peptide as Delivery Systems for Targeted Anti-Cancer Chemotherapy. *Investigational New Drugs* **2019**, *37*, 771–778. https://doi.org/10.1007/s10637-018-0711-9.

53 Mazzaglia, A.; Donohue, R.; Ravoo, B. J.; Darcy, R. Novel Amphiphilic Cyclodextrins: Graft-Synthesis of Heptakis(6-Alkylthio-6-Deoxy)-β-Cyclodextrin 2-Oligo(Ethylene Glycol) Conjugates and Their ω-Halo Derivatives. *Eur. J. Org. Chem.* **2001**, *9*, 1715–1721. https://doi.org/10.1002/1099-0690(200105)2001:9<1715::AID-EJOC1715>3.0.CO;2-A.

54 Mineo, P.; Vitalini, D.; Scamporrino, E.; Bazzano, S.; Alicata, R. Effect of Delay Time and Grid Voltage Changes on the Average Molecular Mass of Polydisperse Polymers and Polymeric Blends Determined by Delayed Extraction Matrix-Assisted Laser Desorption/Ionization Time-of-Flight Mass Spectrometry. *Rapid Communications in Mass Spectrometry* **2005**, *19* (19), 2773–2779. https://doi.org/10.1002/rcm.2123.

55 Vitalini, D.; Mineo, P.; Scamporrino, E. Effect of Combined Changes in Delayed Extraction Time and Potential Gradient on the Mass Resolution and Ion Discrimination in the Analysis of Polydisperse Polymers and Polymer Blends by Delayed Extraction Matrix-Assisted Laser Desorption/Ionization Time-of-Flight Mass Spectrometry. *Rapid Communications in Mass Spectrometry* **1999**, *13* (24), 2511–2517. https://doi.org/10.1002/(SICI)1097-0231(19991230)13:24<2511::AID-RCM819>3.0.CO;2-Y.

56 Scamporrino, E.; Vitalini, D.; Mineo, P. Synthesis and MALDI-TOF MS Characterization of High Molecular Weight Poly(1,2-dihydroxybenzene phthalates) Obtained by Uncatalyzed Bulk Polymerization of *O,O'*-Phthalid-3-ylidenecatechol or 4-Methyl-*O,O'*-phthalid-3-ylidenecatechol. *Macromolecules* **1996**, *29* (17), 5520–5528. https://doi.org/10.1021/ma960051+.

57 Pedersen, S. L.; Tofteng, A. P.; Malik, L.; Jensen, K. J. Microwave Heating in Solid-Phase Peptide Synthesis. *Chem. Soc. Rev.* **2012**, *41* (5), 1826–1844. https://doi.org/10.1039/c1cs15214a

58 Subiros-Funosas, R.; Acosta, G. A.; El-Faham, A.; Albericio, F. Microwave Irradiation and COMU: A Potent Combination for Solid-Phase Peptide Synthesis. *Tetrahedron Letters* **2009**, *50* (45), 6200–6202. https://doi.org/10.1016/j.tetlet.2009.08.117.

59 Ravoo, B. J.; Darcy, R. Cyclodextrin Bilayer Vesicles. *Angew Chem Int Ed Engl* **2000**, *39* (23), 4324–4326. https://doi.org/10.1002/1521-3773(20001201)39:23<4324::AID-ANIE4324>3.0.CO;2-O.

60 Valle, F.; Tortorella, S.; Scala, A.; Cordaro, A.; Barbalinardo, M.; Biscarini, F.; Mazzaglia, A. Amphiphilic Cationic Cyclodextrin Nanovesicles: A Versatile Cue for Guiding Cell Adhesion. *Nanoscale Advances* **2020**, *2* (12), 5897–5904. https://doi.org/10.1039/d0na00623h.

61 Riminucci, A.; Uhlarz, M.; De Santis, R.; Herrmannsdörfer, T. Analytical Balance-Based Faraday Magnetometer. *Journal of Applied Physics* **2017**, *121* (9), 094701. https://doi.org/10.1063/1.4977719.

62 Villari, V.; Micali, N. Light Scattering as Spectroscopic Tool for the Study of Disperse Systems Useful in Pharmaceutical Sciences. *Journal of Pharmaceutical Sciences* **2008**, *97* (5), 1703–1730. https://doi.org/10.1002/jps.21067.

63 Hussain, M. Z.; Linden, B. van der; Yang, Z.; Jia, Q.; Chang, H.; Fischer, R. A.; Kapteijn, F.; Zhu, Y.; Xia, Y. Bimetal–Organic Framework Derived Multi-Heterostructured TiO2/CuxO/C Nanocomposites with Superior Photocatalytic H2 Generation Performance. *J. Mater. Chem. A* **2021**, *9* (7), 4103–4116. https://doi.org/10.1039/d0ta10853g.

64 Sun, S.; Xiong, X.; Han, J.; Chang, X.; Wang, N.; Wang, M.; Lei, Y.; Liu, T.; Zhu, Y. 2D/2D Graphene Nanoplatelet–Tungsten Trioxide Hydrate Nanocomposites for Sensing Acetone. *ACS Appl. Nano Mater.* **2019**, *2* (3), 1313–1324. https://doi.org/10.1021/acsanm.8b02185.

65 Slavov, L.; Abrashev, M. V.; Merodiiska ,T.; Gelev, Vandenberghe R.E.; Markova-Deneva, I.; Nedkov, I. Raman spectroscopy investigation of magnetite nanoparticles in ferrofluids. *Journal of Magnetism and Magnetic Materials*, **2010**, *322*, 1904–1910. https://doi.org/10.1016/j.jmmm.2010.01.005.

66 Karakoti, A. S.; Das, S.; Thevuthasan, S.; Seal, S. PEGylated Inorganic Nanoparticles. *Angew Chem, Int. Ed. Engl.* **2011**, *50* (9), 1980–1994. https://doi.org/10.1002/anie.201002969.

67 Chalasani, R.; Vasudevan, S. Cyclodextrin Functionalized Magnetic Iron Oxide Nanocrystals: A Host-Carrier for Magnetic Separation of Non-Polar Molecules and Arsenic from Aqueous Media. *J. Mater. Chem.* **2012**, *22* (30), 14925–14931. https://doi.org/10.1039/c2jm32360e.

68 Amstad, E.; Textor, M.; Reimhult, E. Stabilization and Functionalization of Iron Oxide Nanoparticles for Biomedical Applications. *Nanoscale* **2011**, *3* (7), 2819–2843. https://doi.org/10.1039/c1nr10173k.

69 Schenkel, J. H.; Samanta, A.; Ravoo, B. J. Self-Assembly of Soft Hybrid Materials Directed by Light and a Magnetic Field. *Adv. Mater.* **2014**, *26* (7), 1076–1080. https://doi.org/10.1002/adma.201304689.

70 Nowak, B. P.; Ravoo, B. J. Magneto- and Photo-Responsive Hydrogels from the Co-Assembly of Peptides, Cyclodextrins, and Superparamagnetic Nanoparticles. *Faraday Discuss.* **2019**, *219* (0), 220–228. https://doi.org/10.1039/c9fd00012g.

71 Wagner, C. D.; Naumkin, A. V.; Kraut-Vass, A.; Allison, J. W.; Powell, C. J.; Rumble Jr. J. R. NIST Standard Reference Database 20, Version 3.4, (2003) http://srdata.nist.

72 Bozzi, A.; Yuranova, T.; Mielczarski, J.; Kiwi, J. Evidence for Immobilized Photo-Fenton Degradation of Organic Compounds on Structured Silica Surfaces Involving Fe Recycling. *New J. Chem.* **2004**, *28* (4), 519–526. https://doi.org/10.1039/B316027K.

73 Casaletto, M. P.; Figà, V.; Privitera, A.; Bruno, M.; Napolitano, A.; Piacente, S. Inhibition of COR-TEN Steel Corrosion by " Green " Extracts of Brassica Campestris. *Corrosion Science* **2018**, *136*. https://doi.org/10.1016/j.corsci.2018.02.059.

74 Giuffrida, M. L.; Tomasello, M. F.; Pandini, G.; Caraci, F.; Battaglia, G.; Busceti, C.; Di Pietro, P.; Pappalardo, G.; Attanasio, F.; Chiechio, S.; Bagnoli, S.; Nacmias, B.; Sorbi, S.; Vigneri, R.; Rizzarelli, E.; Nicoletti, F.; Copani, A. Monomeric β-Amyloid Interacts with Type-1 Insulin-like Growth Factor Receptors to Provide Energy Supply to Neurons. *Front. Cell. Neurosci.* **2015**, *9*. 297. https://doi.org/10.3389/fncel.2015.00297.

TOC